





The pathogenic R5L mutation disrupts formation of Tau complexes on the microtubule by altering local N-terminal structure

Alisa Cario^a, Adriana Savastano^b, Neil B. Wood^a, Zhu Liu^c, Michael J. Previs^a, Adam G. Hendricks^c , Markus Zweckstetter^{b,d} , and Christopher L. Berger^{a,1} 

^aDepartment of Molecular Physiology and Biophysics, University of Vermont, Burlington, VT 05405; ^bResearch Group Translational Structural Biology, German Center for Neurodegenerative Diseases, Göttingen 37075, Germany; ^cDepartment of Bioengineering, McGill University, Montréal, QC H3A 0C3, Canada; and ^dDepartment for NMR-Based Structural Biology, Max Planck Institute for Biophysical Chemistry 37077 Göttingen, Germany

Edited by Cyrus Safinya, Materials, Physics, and Molecular, Cellular, and Developmental Biology, University of California, Santa Barbara, CA; received August 12, 2021; accepted December 27, 2021 by Editorial Board Member Yale E. Goldman

The microtubule-associated protein (MAP) Tau is an intrinsically disordered protein (IDP) primarily expressed in axons, where it functions to regulate microtubule dynamics, modulate motor protein motility, and participate in signaling cascades. Tau misregulation and point mutations are linked to neurodegenerative diseases, including progressive supranuclear palsy (PSP), Pick's disease, and Alzheimer's disease. Many disease-associated mutations in Tau occur in the C-terminal microtubule-binding domain of the protein. Effects of C-terminal mutations in Tau have led to the widely accepted disease-state theory that missense mutations in Tau reduce microtubule-binding affinity or increase Tau propensity to aggregate. Here, we investigate the effect of an N-terminal arginine to leucine mutation at position 5 in Tau (R5L), associated with PSP, on Tau–microtubule interactions using an *in vitro* reconstituted system. Contrary to the canonical disease-state theory, we determine that the R5L mutation does not reduce Tau affinity for the microtubule using total internal reflection fluorescence microscopy. Rather, the R5L mutation decreases the ability of Tau to form larger-order complexes, or Tau patches, at high concentrations of Tau. Using NMR, we show that the R5L mutation results in a local structural change that reduces interactions of the projection domain in the presence of microtubules. Altogether, these results challenge both the current paradigm of how mutations in Tau lead to disease and the role of the projection domain in modulating Tau behavior on the microtubule surface.

Tau | microtubule | neurodegenerative diseases | TIRF microscopy | NMR spectroscopy

The microtubule-associated protein (MAP) Tau is an intrinsically disordered protein (IDP) highly expressed in the axon, where it functions to regulate microtubule dynamics (1, 2), modulate motor protein motility (3–6), and participate in signaling cascades (7, 8). Misregulation and aggregation of Tau are linked to a number of neurodegenerative diseases known as Tauopathies. These include Alzheimer's disease, frontotemporal dementia, and progressive supranuclear palsy (PSP) (9–13). Disease-associated perturbations to Tau, including hyperphosphorylation, are generally thought to initiate the disease state by decreasing the affinity for microtubules (14–16). In support, there are over 50 disease-associated mutations in Tau and many have been shown to either reduce Tau affinity for the microtubule (17, 18) or promote Tau aggregation (18). However, many of the studied alterations are within the regions of Tau that directly bind to the microtubule, and less is understood about disease-associated mutations outside of the microtubule-binding region of Tau.

There are six isoforms of Tau expressed in the human brain (19), and although the exact composition can vary dependent on alternative splicing (20–22), all share the same functional domains. Three or four imperfect microtubule-binding repeats

directly interface with the microtubule (23–28) in an extended conformation along a single protofilament (29), largely contributing to the high affinity of Tau for the microtubule. Adjacent to the microtubule-binding repeats is the proline-rich region, which helps mediate microtubule binding (24, 27, 28, 30). The structurally flexible N-terminal region of Tau, known as the projection domain, contains alternatively spliced acidic inserts (zero, one, or two) and has the lowest contribution to the overall binding affinity of Tau for the microtubule (23, 31).

Additionally, Tau interaction with the microtubule is complicated by multiple binding modes. Tau binding is concentration dependent. At low concentrations, Tau binds to the microtubule in a dynamic equilibrium between static and diffusive binding states (32, 33). However, as the concentration of Tau increases, Tau binds nonuniformly and forms larger-order complexes, referred to as Tau patches (6), Tau cohesive islands (34), or Tau condensates (35). Tau complex formation on the microtubule is not restricted to *in vitro* studies as microtubule-bound complexes have been seen in neurons and other cell types (35–37). Interestingly, in addition to the clear role for the C-terminal microtubule-binding region of Tau in complex formation, the

Significance

The microtubule-associated protein Tau is strongly linked to a number of neurological diseases. Disease onset is typically associated with weakened interaction with the microtubule, but this widely accepted model is based on hyperphosphorylation or mutations within the C-terminal microtubule-binding domain of Tau. Here, we find that an N-terminal disease-associated mutation in Tau, R5L, does not reduce Tau affinity for microtubules but instead, modifies the N-terminal structure, altering Tau's behavior and ability to condense on the microtubule surface. Our findings challenge the current paradigms of both how mutations in Tau lead to disease and the functional role of the N-terminal region of Tau.

Author contributions: A.C., M.Z., and C.L.B. designed research; A.C. and A.S. performed research; N.B.W., Z.L., and M.J.P. contributed new reagents/analytic tools; A.C., A.S., N.B.W., Z.L., M.J.P., A.G.H., and C.L.B. analyzed data; and A.C., A.S., A.G.H., M.Z., and C.L.B. wrote the paper.

The authors declare no competing interest.

This article is a PNAS Direct Submission. C.S. is a guest editor invited by the Editorial Board.

This article is distributed under [Creative Commons Attribution-NonCommercial-NoDerivatives License 4.0 \(CC BY-NC-ND\)](https://creativecommons.org/licenses/by-nc-nd/4.0/).

See [online](#) for related content such as Commentaries.

¹To whom correspondence may be addressed. Email: cberger@uvm.edu.

This article contains supporting information online at <http://www.pnas.org/lookup/suppl/doi:10.1073/pnas.2114215119/-DCSupplemental>.

Published February 8, 2022.

N-terminal projection domain has been shown to be necessary in Tau cohesive island formation (34).

Although many of the mutations in Tau are found within the C-terminal half of the protein, disease-associated mutations also occur in the N-terminal projection domain, specifically the mutations at arginine 5 (R5L, R5H) associated with PSP (38). The R5L (arginine to leucine) mutation has been shown to reduce microtubule assembly, although the mechanism behind this change is unclear (39, 40). It has been shown that deletion of the projection domain does not reduce Tau affinity for the microtubule (26, 41, 42) but is necessary for Tau complex formation (34). Thus, we hypothesize that the N-terminal disease-associated mutation R5L alters Tau binding behavior on the microtubule, disrupting patch formation without altering Tau affinity. Our results suggest the R5L mutation is unlike other disease-associated mutations and alters Tau–microtubule interactions in a previously unreported manner, leading to insight into a potential disease mechanism.

Results

R5L-Tau Reduces Occupancy but Does Not Alter Affinity on Taxol Microtubules. To study the effect of R5L-Tau on Tau–microtubule interactions, the R5L mutation was cloned into the 3RS isoform of Tau (R5L-Tau) and the affinity of R5L-Tau was assessed relative to wild-type Tau (WT-Tau) using a TIRF (total internal reflection fluorescence) microscopy binding assay as previously reported (43). Fluorescently labeled Tau (10 to 400 nM WT-Tau or R5L-Tau) was incubated with microtubules stabilized with paclitaxel (Taxol microtubules) (Fig. 1A). The average Tau intensity on the microtubule was plotted against the Tau concentration (Fig. 1B). It was determined that the R5L mutation did not significantly alter the affinity of Tau for Taxol microtubules (WT-Tau $K_D = 277 \pm 30$ nM, R5L-Tau $K_D = 261 \pm 29$ nM) (Fig. 1B).

Interestingly, the TIRF binding assay revealed a twofold difference in fluorescence intensity between WT-Tau and R5L-Tau at binding saturation, despite similar affinities (Fig. 1B). It was determined that this was not due to a difference in labeling efficiency, which was determined by a modified Lowry assay in conjunction with absorbance measurements or through liquid chromatography–mass spectrometry (*SI Appendix, Methods*) or quenching of the fluorescent probe (*SI Appendix, Fig. S9*). Therefore, we hypothesized that the R5L mutation reduces the occupancy of Tau on microtubules without altering affinity,

leading to less Tau bound to microtubules at binding saturation. To test this hypothesis, a microtubule pelleting assay was performed by incubating 100 nM labeled WT-Tau or R5L-Tau with varying concentrations of Taxol microtubules (50 nM to 1 μ M). The relative amount of Tau bound to Taxol microtubules was assessed by measuring the fluorescence in the supernatant relative to the pellet. At saturating conditions, less R5L-Tau bound to microtubules compared with WT-Tau (Fig. 1C).

The R5L Mutation Disrupts Tau Patch Formation. The TIRF binding assays also showed nonuniform binding of Tau along the microtubule as the concentration increased (Fig. 1A and *Movies S1* and *S2*). This is consistent with other reports of Tau forming larger-order complexes on the microtubule surface, known as Tau patches, cohesive islands, or condensates (6, 32, 33, 35). Therefore, we studied the effect of the R5L mutation on Tau patches by incubating 250 nM Tau (WT-Tau or R5L-Tau) with Taxol microtubules using TIRF microscopy (Fig. 2A). Patch frequency was quantified as the number of patches per unit length along the microtubule. WT-Tau formed twice as many patches per micrometer compared with R5L-Tau (WT-Tau = 0.36 ± 0.21 , R5L-Tau = 0.18 ± 0.21) (Fig. 2B). WT-Tau patches also contained ~50% more molecules than R5L-Tau patches (WT-Tau = 3.3 ± 1.1 molecules per patch, R5L-Tau = 2.1 ± 1.8 molecules per patch) (Fig. 2C). Furthermore, we examined the fluorescence intensity distribution along the microtubule (Fig. 2D). There was a higher mean fluorescence intensity and a broader distribution for WT-Tau compared with R5L-Tau. Thus, WT-Tau forms more numerous and larger patches compared with R5L-Tau.

R5L-Tau Shifts Binding Behavior at High Concentrations on Taxol Microtubules. We investigated the difference in the binding behavior of individual R5L-Tau and WT-Tau molecules on Taxol microtubules using TIRF microscopy. Previous work has shown that at low concentrations of Tau, Tau binds to the microtubule in a dynamic equilibrium between static and diffusive binding states (32, 33). Therefore, we studied the binding behavior of 500 pM WT-Tau or R5L-Tau bound to Taxol microtubules and measured the binding-state equilibrium, diffusion coefficient, and dwell times of both static and diffusive events (representative kymographs are shown in *SI Appendix, Fig. S1*). There was no significant difference in the binding-state equilibrium at this low concentration of WT-Tau and R5L-Tau, with approximately half

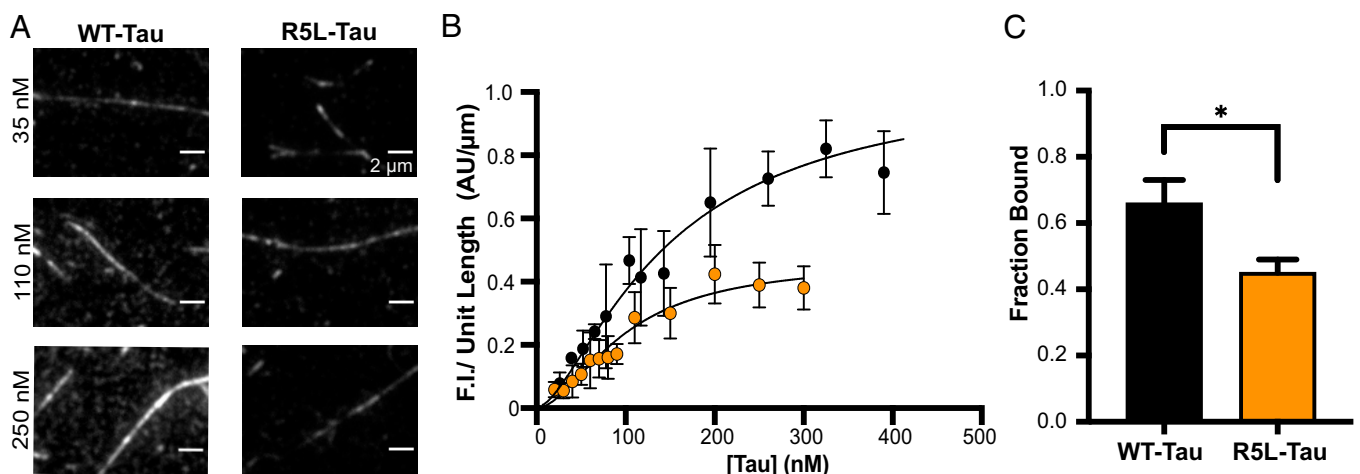


Fig. 1. The R5L mutation reduces Tau occupancy on Taxol microtubules. (A) Representative images of WT-Tau (Left) and R5L-Tau (Right) decoration of Taxol microtubules at varying Tau concentrations. (B) TIRF-based binding assays, measuring fluorescence intensity (F.I.) in arbitrary units (AU) normalized to microtubule length (μ m), comparing WT-Tau (black; $K_D = 277 \pm 30$ nM) and R5L-Tau (orange; $K_D = 261 \pm 29$ nM). Data are mean \pm 95% CI ($n = 4$). (C) Microtubule pelleting assay comparing relative fluorescence-bound Tau of WT-Tau (black; 0.66 ± 0.07) or R5L-Tau (orange; 0.45 ± 0.04) at 100 nM Tau and 1 μ M Taxol microtubules. Data are mean \pm SD ($n = 3$). Statistical analysis was performed using the Student's *t* test. * $P < 0.05$.

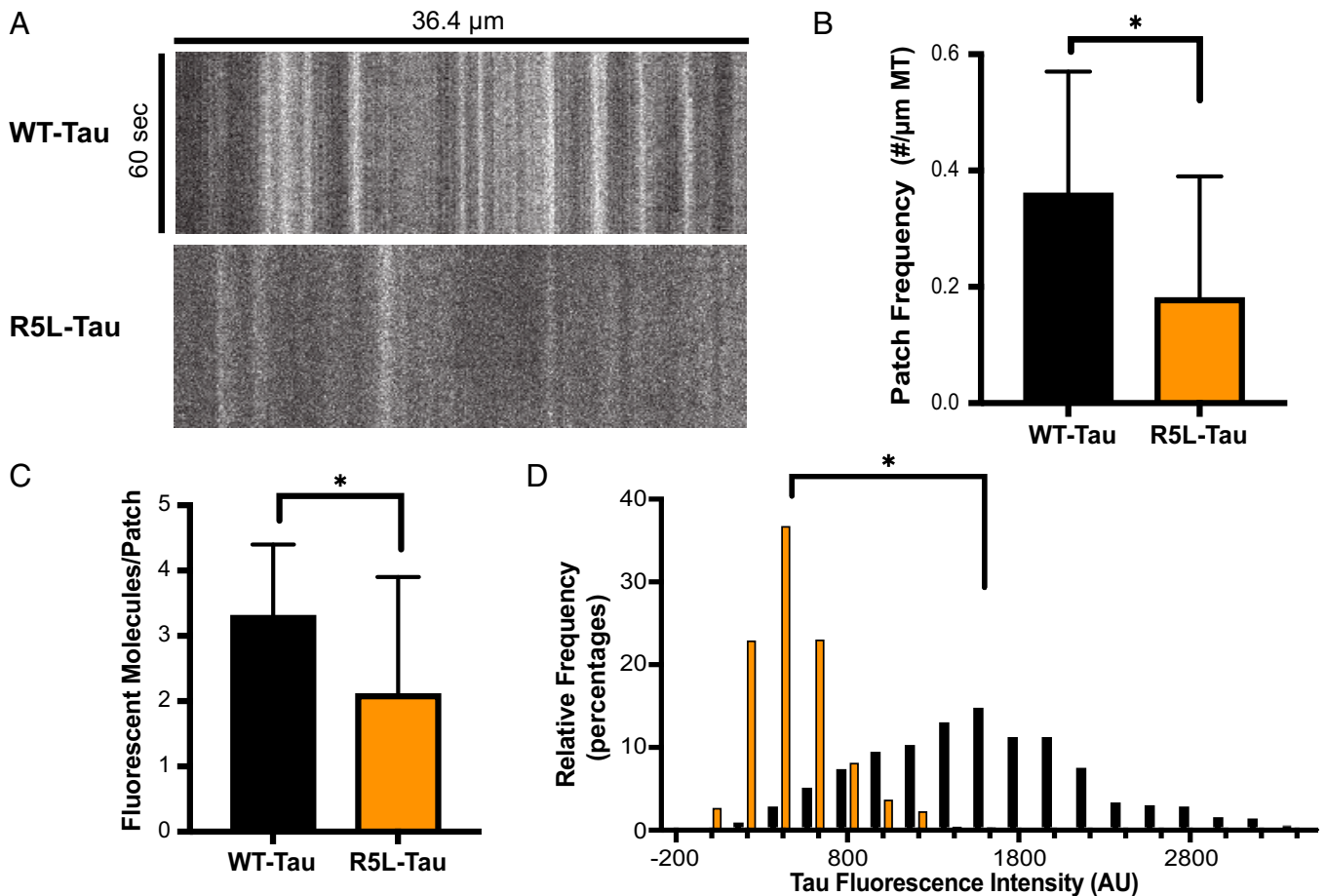


Fig. 2. The R5L mutation alters Tau patches on Taxol microtubules. Tau patches were studied using 250 nM Alexa 488 Tau on Taxol microtubules. (A) Representative kymographs of WT-Tau (Upper) and R5L-Tau (Lower) at 250 nM Tau concentration. (B) Patch frequency of WT-Tau (black; 0.36 ± 0.21 patches per $1 \mu\text{m}$ microtubule [MT]) and R5L-Tau (orange; 0.18 ± 0.21 patches per $1 \mu\text{m}$ MT). Data are mean \pm SD ($n = 80$ kymographs). Statistical analysis was performed using the Student's t test. $*P < 0.05$. (C) Number of fluorescent molecules per patch of WT-Tau (black; 3.3 ± 1.1 fluorescent molecules per patch) and R5L-Tau (orange; 2.1 ± 1.8 fluorescent molecules per patch). Data are mean \pm SD ($n = 80$ kymographs). Statistical analysis was performed using the Student's t test. $*P < 0.05$. (D) Histograms of normalized WT-Tau (black) and R5L-Tau (orange) Tau fluorescence intensity on microtubules. Values above 1% are shown ($n = 80$ kymographs). Statistical analysis was performed using the Mann-Whitney test. $*P < 0.01$.

of the binding events observed in the static state (Table 1 and *SI Appendix, Fig. S2*). Additionally, the R5L mutation had little effect on the diffusion coefficient or dwell time of individual molecules in either the static or diffusive states (Table 1 and *SI Appendix, Figs. S3 and S4*). Overall, these data showed little difference in the binding behavior between WT-Tau and R5L-Tau at low concentrations.

However, at higher Tau concentrations, complexes composed of statically bound Tau molecules form on the microtubule (35). Due to the differences in R5L-Tau patch formation, we examined the binding behavior of individual Tau molecules at high concentrations by performing a spiking experiment where either 250 or 500 nM Alexa 488 WT-Tau or R5L-Tau was spiked with 300 pM Alexa 647 Tau (*Movies S3 and S4*). We examined the static-diffusive equilibrium, diffusion coefficient, and dwell times. At high concentrations of Tau, both 250 and 500 nM Tau, there was a shift toward diffusive binding for R5L-Tau. At 250 nM Tau, 48% of WT-Tau bound statically compared with 17% for R5L-Tau (Table 1 and *SI Appendix, Fig. S2*). At 500 nM, 54% of WT-Tau bound statically compared with 29% for R5L-Tau (Table 1 and *SI Appendix, Fig. S2*). There was little overall difference in the diffusion coefficients or dwell times of either static or diffusive molecules at higher Tau concentrations (Table 1 and *SI Appendix, Figs. S3 and S4*). Thus, at high concentrations R5L-Tau shifts to a predominantly diffusive state (Table 1).

R5L-Tau Reduces Occupancy but Does Not Alter Affinity on Guanosine 5'-[(α,β)-Methylene] Triphosphate Sodium Salt Microtubules. On Taxol microtubules, the R5L mutation had two effects: less Tau bound to the microtubule and fewer Tau patches. However, it was unclear if these two effects of the R5L mutation were linked. Previous work from our laboratory has shown that in comparison with Taxol microtubules, Tau binds as single molecules and does not form complexes on microtubules stabilized with guanosine 5'-[(α,β)-methylene] triphosphate sodium salt (GMPCPP) microtubules (33). Consistent with these data, recent work shows that Tau condensates do not form on GMPCPP microtubules (35). Therefore, we studied R5L-Tau binding to GMPCPP microtubules to examine the effect of the R5L mutation independent of patch formation. The TIRF binding assay indicated that, as expected, both WT-Tau and R5L-Tau had a lower affinity for GMPCPP microtubules compared with Taxol microtubules (44, 45). However, there was little difference in affinity between WT-Tau and R5L-Tau (WT-Tau $K_D = 564 \pm 100$ nM, R5L-Tau $K_D = 515 \pm 149$ nM) (Fig. 3B and *Movies S5 and S6*). Interestingly, there was a lower fluorescence intensity at saturation with R5L-Tau compared with WT-Tau (Fig. 3B). Microtubule pelleting assays confirmed that less R5L-Tau bound to GMPCPP microtubules compared with WT-Tau (Fig. 3C).

Table 1. Summary of WT-Tau and R5L-Tau behavior on microtubules

	Static, %	Diffusion coefficient, $\mu\text{m}^2/\text{s}$	Dwell time static, s	Dwell time diffusive, s
Taxol				
500 pM				
WT-Tau	45	0.29 ± 0.04	1.5 ± 0.3	1.4 ± 0.1
R5L-Tau	57	0.33 ± 0.04	1.6 ± 0.2	1.2 ± 0.2
250 nM				
WT-Tau	48	0.14 ± 0.02	1.8 ± 0.4	2.4 ± 0.3
R5L-Tau	17*	$0.21 \pm 0.02^*$	2.1 ± 0.3	2.3 ± 0.2
500 nM				
WT-Tau	54	0.16 ± 0.03	1.5 ± 0.3	1.3 ± 0.3
R5L-Tau	29*	0.18 ± 0.02	1.6 ± 0.2	$1.9 \pm 0.3^*$
GMPCPP				
500 pM				
WT-Tau	26	0.75 ± 0.10	2.2 ± 0.5	1.1 ± 0.2
R5L-Tau	23	0.75 ± 0.10	$1.0 \pm 0.2^*$	0.9 ± 0.1
400 nM				
WT-Tau	15	0.50 ± 0.08	2.0 ± 0.6	1.5 ± 0.4
R5L-Tau	14	0.44 ± 0.09	1.1 ± 0.1	1.2 ± 0.1

Low-concentration studies were performed with 500 pM Alexa 647-labeled Tau on microtubules. For Taxol microtubules, high-concentration studies were performed through a spiking experiment, incubating either 250 or 500 nM Alexa 488-labeled Tau with 300 pM Alexa 647-labeled Tau. For GMPCPP microtubules, high-concentration studies were performed through a spiking experiment, incubating 400 nM Alexa 488-labeled Tau with 300 pM Alexa 647-labeled Tau. Static:Diffusive equilibrium is represented as percent static molecules. Statistical analysis was performed using the Fisher's Exact test relative to WT-Tau under the same conditions. * $P < 0.01$. Dwell times and diffusion coefficients are represented as medians \pm 95% CIs. Statistical analysis was performed using the Mann-Whitney test relative to WT-Tau under the same conditions. * $P < 0.01$.

The R5L Mutation Does Not Alter Binding Behavior on GMPCPP Microtubules. To further understand the effect of R5L-Tau on GMPCPP microtubules, we studied the binding behavior at low concentrations of Tau (500 pM WT-Tau or R5L-Tau) (Table 1). At 500 pM, both WT-Tau and R5L-Tau shift toward diffusive binding on GMPCPP microtubules, consistent with previous work from our laboratory (33), but there was no significant difference in the overall binding behavior of WT-Tau vs. R5L-Tau. Twenty-six percent of WT-Tau bound in the static state compared with 23% of R5L-Tau (Table 1 and *SI Appendix, Fig. S6*), and there was no difference in diffusion coefficient or diffusive dwell time. However, when bound statically, WT-Tau had a

higher dwell time compared with R5L-Tau (WT-Tau = 2.2 ± 0.5 s, R5L-Tau = 1.0 ± 0.2 s) (Table 1 and *SI Appendix, Figs. S7 and S8*).

A shift in binding behavior for R5L-Tau occurred at high concentrations on Taxol microtubules (Table 1 and *SI Appendix, Fig. S2*). Therefore, we studied the binding behavior at high concentrations of Tau on GMPCPP microtubules by performing a spiking experiment where we incubated 400 nM Alexa 488 WT-Tau or R5L-Tau spiked with 300 pM Alexa 647 Tau to visualize individual molecules on GMPCPP microtubules (Table 1; representative kymographs are shown in *SI Appendix, Fig. S5*). At 400 nM Tau, 15% of WT-Tau bound statically compared

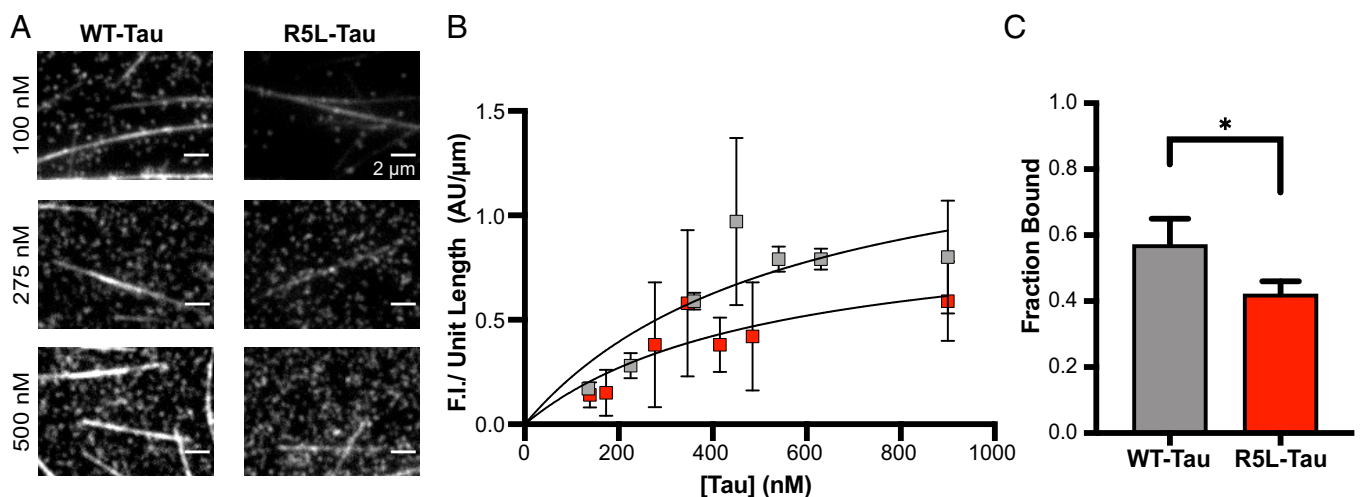


Fig. 3. The R5L mutation reduces occupancy on GMPCPP microtubules. (A) Representative images of WT-Tau (Left) and R5L-Tau (Right) decoration of GMPCPP microtubules at varying Tau concentrations. (B) TIRF-based binding assays, measuring fluorescence intensity (F.I.) in arbitrary units (AU) normalized to microtubule length (μm), comparing WT-Tau (gray; $K_D = 564 \pm 100$ nM) and R5L-Tau (red; 515 ± 149 nM). Data are mean \pm 95% CI ($n = 4$). (C) Microtubule pelleting assay comparing relative fluorescence-bound Tau of 300 nM WT-Tau (gray; 0.57 ± 0.08) or R5L-Tau (red; 0.42 ± 0.04) bound to 1 μM GMPCPP microtubules. Data are mean \pm SD ($n = 3$). Statistical analysis was performed using the Student's t test. * $P < 0.05$.

with 14% of R5L-Tau (Table 1 and *SI Appendix*, Fig. S6). Similar to low concentrations of Tau, there was little difference in the diffusion coefficient or diffusive dwell time (Table 1 and *SI Appendix*, Figs. S7 and S8). However, WT-Tau had a higher dwell time compared with R5L-Tau (WT-Tau = 2.0 ± 0.6 s, R5L-Tau = 1.1 ± 0.1 s) in the static state (Table 1 and *SI Appendix*, Fig. S8), albeit that this is a small percentage of the total binding events. Contrary to Taxol microtubules, we did not see any significant differences in binding behavior on GMPCPP microtubules at high concentrations of Tau.

The R5L Mutation Alters the Local Structure of Tau. We then examined the impact of the R5L mutation on the secondary structure and global conformation of Tau using circular dichroism (CD) and dynamic light scattering (DLS). Both WT-Tau and R5L-Tau had similar CD spectra, typical for random coil conformation with minima at ~ 200 nm (Fig. 4A) (46), and hydrodynamic radii (R_H) as determined by DLS (Fig. 4A). Two-dimensional (2D) ^1H - ^{15}N heteronuclear single-quantum coherence (HSQC) NMR spectroscopy experiments of $10 \mu\text{M}$ ^{15}N -labeled Tau (WT-Tau or R5L-Tau) were used to obtain residue-specific structural information (47, 48) on the effect of the R5L mutation. Alterations in chemical shift were observed within 5 to 10 residues of the site of mutation, suggesting a local structural change restricted to the first 20 amino acids within the N-terminal projection domain (Fig. 4B–D).

NMR spectra of IDPs like Tau are prone to signal overlap (48). We therefore further investigated the consequences of the R5L mutation using short peptides comprising the first 20 residues (WT-Tau or R5L-Tau) (Fig. 4E and F). Similar to the full-length protein, chemical shift perturbations from natural abundance 2D ^1H - ^{15}N HSQC experiments on 1 mM peptides were observed in direct proximity to the site of mutation (Fig. 4E). The two glutamate residues E3 and E7, which are one residue away from the R5L mutation, showed the largest perturbations (Fig. 4F). The combined analysis demonstrates that the structural changes caused by the R5L mutation are highly local and do not affect the microtubule-binding domain.

The R5L Mutation Causes a Reduction in Projection Domain Interactions with the Microtubule. To investigate the effect of the R5L mutation on the interaction of Tau with microtubules, we recorded 2D ^1H - ^{15}N HSQC experiments of $10 \mu\text{M}$ ^{15}N -labeled WT-Tau or R5L-Tau in the absence or presence of $20 \mu\text{M}$ Taxol microtubules (Fig. 5A). Upon binding to microtubules, the signal intensity of Tau residues interacting with the microtubule surface decreases (25), which can be visualized in an intensity ratio plot (Fig. 5A). The strongest drop in signal intensity is seen for both proteins in the second proline-rich region through the microtubule-binding repeats, which together form the microtubule-binding domain of Tau. In agreement with the highly local nature of the structural perturbations of the R5L mutation (Fig. 4C–F), the R5L mutation does not influence the high-affinity C-terminal microtubule-binding domain of Tau. In contrast, the R5L mutation affects the N-terminal projection domain of Tau. The signal attenuation at the N terminus of R5L-Tau is weaker when compared with WT-Tau (Fig. 5A), which becomes particularly evident upon inspection of the intensity difference plot (Fig. 5A). Notably, while the R5L-induced chemical shift perturbation was restricted to the N-terminal 15 residues in solution (Fig. 4C), the mutation affects up to 50 residues of the projection domain of Tau in the presence of microtubules.

To quantify the effect of the mutation on Tau binding to microtubules, we used saturation transfer difference (STD) NMR spectroscopy, which provides information on the residues involved in the binding with a larger protein (i.e., microtubules) (49–51). The efficiency of saturation transfer was investigated

for the WT-Tau and R5L-Tau peptides in the presence of $5 \mu\text{M}$ Taxol microtubules through the measurement of the STD NMR signals at increasing saturation time. For selected protons (i.e., Y18H δ and A2H β), the STD buildup curve is displayed (Fig. 5B). Notably, we observe a larger effect for Y18H δ when compared with A2H β . We attribute this to the tendency of the aromatic residue Y18H δ to interact with the surface of the microtubule and thus, decrease its interaction with the solvent. The analysis further demonstrates that both peptides receive magnetization from the microtubules, and for selected protons, the saturation transfer is more efficient for the WT-Tau peptide when compared with the R5L-Tau peptide. Subsequently, we determined the microtubule-binding affinity of the two peptides by measuring STD NMR experiments with fixed concentration of Taxol microtubules and gradually increasing peptide concentrations (Fig. 5C). The K_D values obtained for Y18H δ and A2H β of the WT-Tau peptide were 1.3 ± 0.3 and 0.9 ± 0.2 mM, respectively. In case of the R5L-Tau peptide, we derived K_D values of 3.3 ± 1.5 and 2.7 ± 0.4 mM, respectively.

Discussion

Missense mutations and hyperphosphorylation of Tau that leads to neurodegeneration, such as PSP, are generally thought to be initiated by a decrease in Tau's interaction with the microtubule. A reduction in binding affinity has been demonstrated in previously studied disease-associated mutations in the microtubule-binding region (e.g., $\Delta 280\text{K}$, P301L, and V337M) (17, 52–56). However, the present work challenges the generally accepted model of Tauopathies as the R5L mutation, located in the N-terminal projection domain, does not alter Tau affinity for the microtubule. This is consistent with past studies where deletion of the entire projection domain did not reduce Tau affinity (26, 41, 42). Furthermore, microtubule-induced NMR signal broadening measurements show no differences observed between WT-Tau and R5L-Tau signal attenuation within the microtubule-binding region, consistent with no change in affinity. It should be noted that other alterations in the N terminus of Tau, such as phosphorylation of Y18 (43), cause global conformational changes to Tau (7), likely through disruption of transient long-range interactions between the N- and C-terminal domains (31, 48, 57, 58). However, CD, DLS, and NMR indicate no global conformational changes of R5L-Tau relative to WT-Tau in solution, as the R5L mutation only perturbs the local structure of Tau proximal to the mutation (up to ~ 10 amino acids from R5). Additionally, no long-range effects are measured in the presence of microtubules, where changes to the microtubule-induced signal broadening remain local but are propagated ~ 50 residues from the site of the mutation. Thus, the R5L mutation does not alter the global conformational ensemble of Tau or its microtubule-binding affinity.

Tau is known to form complexes on Taxol microtubules, which have been referred to as Tau patches (6), condensates (35), or cohesive islands (34). Similarly, microtubule-bound Tau complexes have been shown to occur in neurons and other cell types (35–37). Although it is not clear whether these complexes are identical as experimental conditions differ, all Tau complexes share similar properties. Our previous work has shown that static Tau forms small complexes on Taxol microtubules (33). Moreover, recent work has shown that Tau condensates/cohesive islands are composed of statically bound molecules (34, 35). Here, TIRF dynamics assays show a concentration-dependent shift in the binding behavior of R5L-Tau on Taxol microtubules, indicating that the R5L mutation disrupts the ability of Tau to form patches. At low concentrations, Tau patches do not form, and there is no difference in the binding behavior between WT-Tau and R5L-Tau. The difference arises

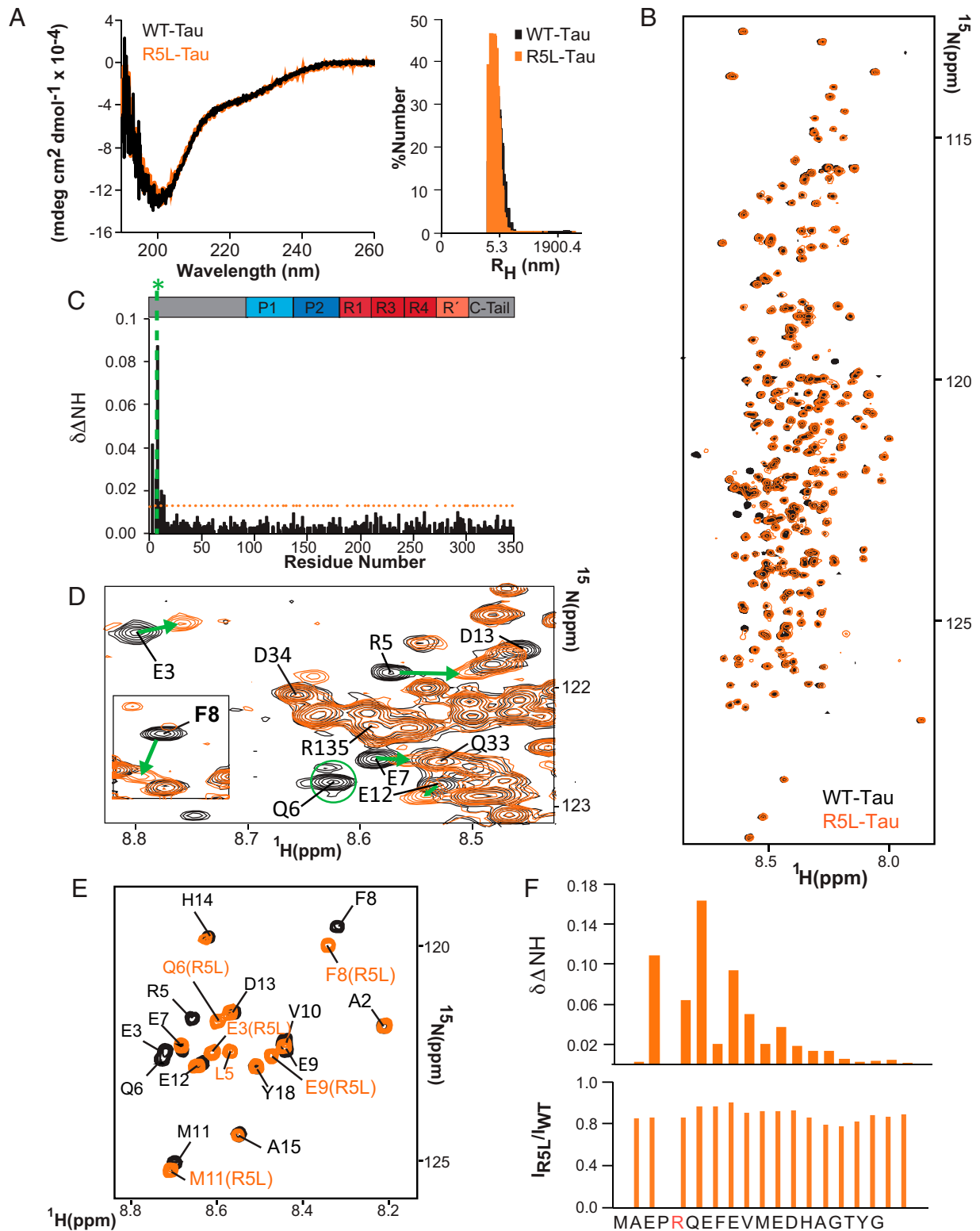


Fig. 4. Changes in the structural dynamics near the R5L mutation of Tau. (A) Structural impact of the R5L mutation probed by CD (Left) and DLS (Right). CD data are reported as mean residue ellipticity for 10 μM samples of WT-Tau and R5L-Tau. (B) Superposition of 2D ^1H - ^{15}N HSQC spectra of WT-Tau (black) and R5L-Tau (orange). (C) Residue-specific ^1H - ^{15}N chemical shift perturbation of Tau upon mutation. The N-terminal region close to the mutated site (indicated by the dashed green line and asterisk) shows chemical shift perturbations above the threshold (the dashed orange line). The threshold was calculated as the SD between all δDNH values [the combined ^1H - ^{15}N chemical shift perturbations calculated according to $(\frac{((\delta\text{H})^2 + (\delta\text{N}/10)^2)}{2})^{1/2}$] and multiplied by a factor of two. The domain organization of Tau is displayed on top of the plot. (D) Zoomed in view of two selected regions of superimposed ^1H - ^{15}N HSQC spectra of WT-Tau (black) and R5L-Tau (orange); shifts are indicated by green arrows. (E and F) NMR characterization of WT-Tau and R5L-Tau peptides (residues 1 to 20 of Tau and R5L-Tau, respectively). (E) Superposition of 2D ^1H - ^{15}N HSQC spectra of Tau (black) and R5L-Tau (orange) peptides. (F) Sequence-specific resonance assignments are indicated. Chemical shift perturbations (Upper) and intensity ratios (Lower) in the R5L-Tau peptide.

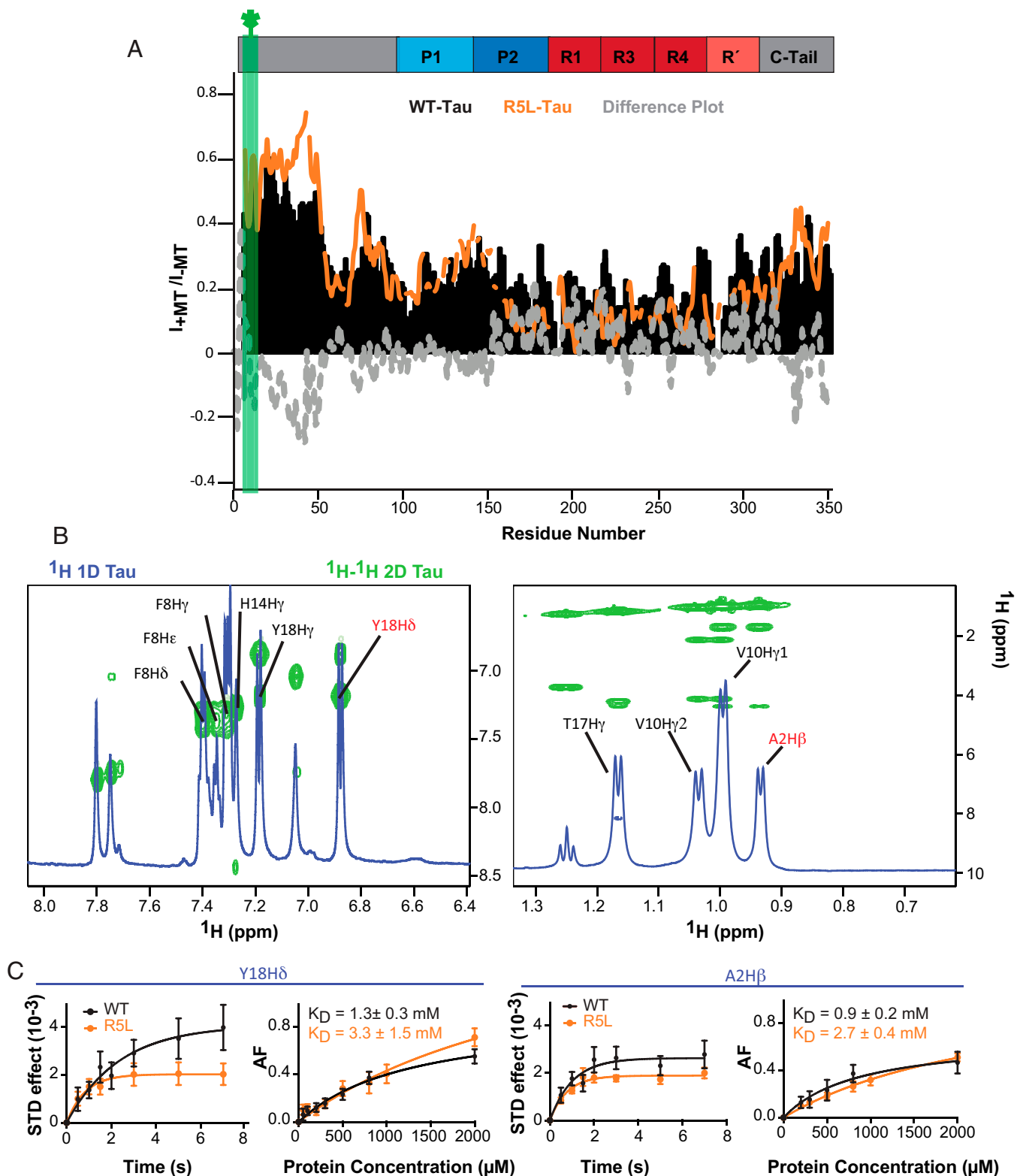


Fig. 5. The R5L mutation attenuates the interaction of the projection domain of Tau in the presence of microtubules. (A) Site-specific changes in the NMR signal intensities of WT-Tau (10 μM ; black bars) or R5L-Tau (10 μM ; orange line) upon addition of 20 μM Taxol microtubules (1:2 molar ratio of Tau:tubulin heterodimer). I_{-MT} and I_{+MT} are the intensities of ^1H - ^{15}N HSQC cross-peaks in the absence and presence of microtubules, respectively. The dashed gray line displays the residue-specific differences between WT-Tau and R5L-Tau. The site of mutation is indicated by the green bar and asterisk. (B) Superposition of the aromatic (Left) and methyl (Right) regions of ^1H one-dimensional and ^1H - ^1H 2D TOCSY spectra of the Tau peptide (residues 1 to 20 of Tau) showing its assignment. The signals of Y18H δ and A2H β (shown in red) were used for further STD NMR analysis. (C) STD effect and K_D values calculated for Y18H δ and A2H β of the N-terminal peptides of WT-Tau (black) and R5L-Tau (orange) for binding to 5 μM Taxol microtubules.

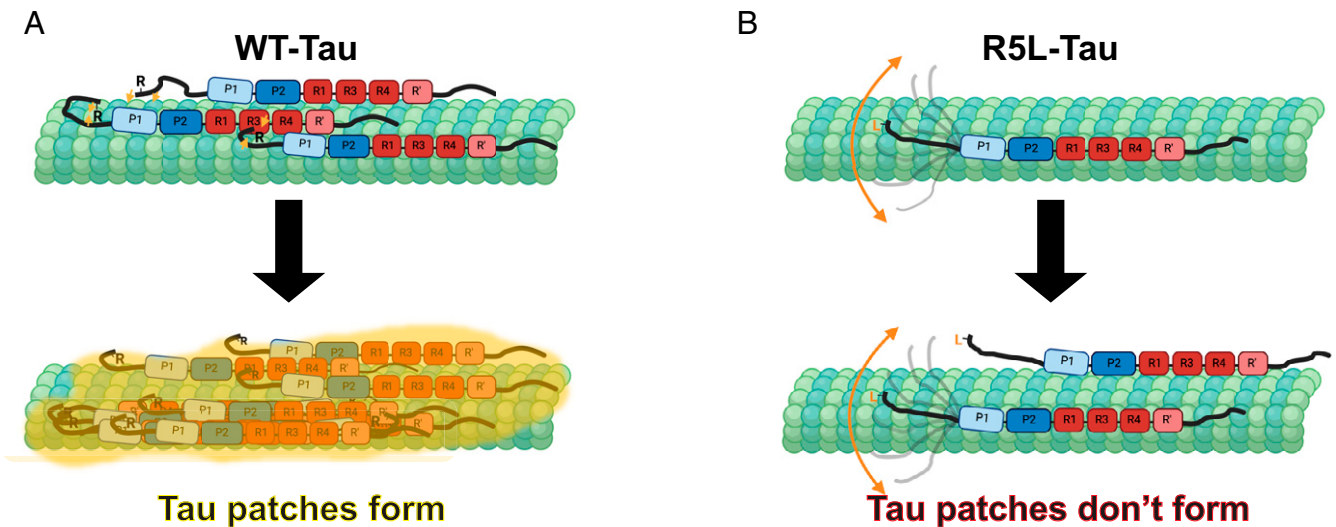


Fig. 6. Mechanistic model for the impact of the R5L mutation on Tau binding to microtubules. The R5L mutation disrupts Tau condensation on the microtubule. (A) The R5 residue is important for salt bridge formation in WT-Tau that does not occur in R5L-Tau. (B) The salt bridge contacts in WT-Tau allow Tau condensation that does not occur in R5L-Tau. Figure created with <https://biorender.com>.

at higher Tau concentrations, where R5L-Tau shifts toward a diffusive state, in agreement with less Tau patch formation (Table 1). Further, R5L-Tau has a lower patch frequency and fewer molecules per patch compared with WT-Tau at high concentrations (Fig. 2 B–D). Our NMR data reveal that the decrease in the frequency and density of Tau patches on the microtubule surface observed by TIRF microscopy is due to changes in the local structure of the projection domain upon introduction of the R5L mutation. Consistent with this finding, previous work has shown that the deletion of the projection domain abolished Tau cohesive islands formation (34). Taken together, this indicates that the projection domain is necessary for microtubule-bound Tau complex formation.

The ability of the R5L mutation to disrupt patch formation is further supported by our work on GMPCPP microtubules, which do not form Tau complexes (33, 35). There is no change in binding behavior between WT-Tau and R5L-Tau on GMPCPP microtubules, supporting that the shift in binding behavior with the R5L mutation on Taxol microtubules is due to disruption of patch formation (Table 1). Interestingly, there is an overall reduction in the occupancy of Tau on GMPCPP microtubules compared with Taxol microtubules, suggesting that a shift toward diffusive binding contributes to the reduced occupancy of R5L-Tau on Taxol microtubules. However, the R5L mutation does not alter the binding-state equilibrium and yet reduces the occupancy on GMPCPP microtubules, indicating that the reduction in occupancy with the R5L mutation is more complicated than a shift in binding behavior and likely due to the local structural changes within the projection domain.

The loss of the arginine residue in R5L-Tau is likely to disrupt one or more important salt bridges, which are known to mediate intermolecular interactions between Tau molecules (59) and between Tau and tubulin (60). However, due to the high flexibility of the projection domain and the corresponding lack of stable structure, the specific salt bridge the R5L mutation disrupts is uncertain. The R5 residue could be engaged in a salt bridge within Tau, with other Tau molecules, or with the microtubule. We hypothesize that the mechanism by which the R5L mutation alters the behavior of microtubule-bound Tau is through loss of a salt bridge involving R5, thus altering the ensemble structural conformations occupied by the projection domain. Our NMR data reveal that the R5L mutation disrupts

the local structure of Tau in solution, which could be attributed to the loss of an intramolecular salt bridge. However, the structural change is enhanced in the presence of microtubules, and therefore, a loss of an intramolecular salt bridge alone does not fully explain how the R5L mutation would lead to disruption of Tau patches. The N-terminal domain of Tau has been shown to be important for intermolecular Tau interactions (61) and the possible formation of an “electrostatic zipper” between Tau molecules (59). Furthermore, the R5L mutation disrupts microtubule-bound Tau complexes, which are suggested to be mediated by intermolecular Tau interactions involving the projection domain (34). Although the overall structure of Tau within a Tau patch remains unclear, disruption on an intermolecular Tau salt bridge between highly acidic projection domains or with the C-terminal binding region of another Tau molecule would lead to disruption of Tau patches. Finally, due to the largely acidic surface of the microtubule, it is feasible that R5 is engaged in a salt bridge with tubulin. Microtubule-induced NMR signal broadening shows a decrease in R5L-Tau N-terminal interactions in the presence of microtubules, suggesting that R5 transiently associates with the microtubule surface. Furthermore, STD measurements of peptides show a reduced affinity with the R5L mutation. Taken together, these experiments show that the R5L mutation weakens the interaction of the projection domain with the microtubule. Our data are consistent with possible interactions of the projection domain with the same microtubule or an adjacent microtubule (62) in densely packed bundles in the axon. These three models are not mutually exclusive, and based on the dynamic nature of Tau, a loss of multiple transient interactions could contribute to the overall effect of the R5L mutation, which is to disrupt microtubule-bound Tau patches (Fig. 6).

Here, we find that the main effect of the disease-associated R5L mutation is disruption of Tau patches, suggesting an important physiological role for microtubule-bound complex formation. Tau functions as a physiological regulator of axonal transport and our results imply direct effects on the ability of R5L-Tau to modulate motor protein motility. Static Tau complexes are known to modulate the motility of kinesin-1 (KIF5C), acting as “roadblocks” on the microtubule (4, 6, 33, 34, 43, 63, 64). Additionally, Tau condensates have been shown to reduce motility of dynein (35). Due to fewer static Tau patches and a reduction in occupancy, we hypothesize that

R5L-Tau is less inhibitory of kinesin-1 and dynein motility compared with WT-Tau. In contrast, diffusive Tau affects the motility of kinesin-3 (KIF1A) (65). Therefore, we would expect that R5L-Tau is more inhibitory to KIF1A motility compared with WT-Tau. However, it is also possible that structural changes in the projection domain could allow R5L-Tau to directly interact with motor proteins, which has been shown for other MAPs (66, 67). Altogether, our data suggest that disruption of Tau patches alters physiological cargo transport and is an intriguing area of future investigation.

This work has additional implications on the ability of R5L-Tau to regulate microtubules. Previous work has shown that, compared with WT-Tau, R5L-Tau reduces total microtubule assembly measured by absorbance at 350 nm (39, 40). The reduction in absorbance could be attributed to a loss of individual microtubule assembly or bundling. The projection domain has a known role in regulating the spacing of microtubule bundles (68), and thus, the R5L mutation could reduce Tau-induced microtubule bundling. However, the role of Tau patch formation on microtubule regulation is unknown. It is possible that Tau patches are important for microtubule stabilization, which is another interesting avenue of future study.

Finally, our data have implications for pathological Tau. It is proposed that the disease state in many Tauopathies is initiated by promoting Tau aggregation and/or reducing Tau affinity for the microtubule. Aggregation of hyperphosphorylated Tau is a hallmark of Tauopathies, such as PSP, and structural changes to the projection domain could alter the phosphorylation state or aggregation propensity of R5L-Tau. Although there are some putative phosphorylation sites in the N-terminal region around the R5 residue (69), NMR experiments show no global conformational change in R5L-Tau. Therefore, it is unlikely that overall phosphorylation patterns are affected by the mutation. Furthermore, studies of the aggregation propensity of R5L-Tau show no large effect of the mutation (39, 70, 71). In this work, we also show that the R5L mutation, unlike other disease-associated mutations, does not reduce Tau affinity for the microtubule. Rather, through a local structural change in the projection domain, the R5L mutation disrupts Tau patch formation, suggesting that Tau patch formation is required for normal Tau function. Therefore, we hypothesize that the mechanism by which the R5L mutation leads to disease is through disruption of physiological Tau function, such as cargo transport, which has been shown to be regulated by Tau complexes (6, 34, 35). Overall, this work challenges the current paradigm of Tauopathies and provides insight into the role of the N-terminal projection domain in modulating normal and pathological states of Tau on the microtubule surface.

Materials and Methods

Purification of Proteins. Tau constructs were purified, characterized, and fluorescently labeled as described (33). Enrichment of ^{15}N Tau was performed as

described (25). Tubulin was purified from bovine brain (72) and polymerized as described (33). Unless otherwise noted, purified proteins were maintained in Brinkley Renaturing Buffer 80 (BRB80; 80 mM PIPES, 1 mM MgCl_2 , 1 mM EGTA, pH 6.9). *SI Appendix, Supplementary Information Text* has details.

Microtubule Pelleting Assay. Microtubule pelleting assays were developed based on Charafeddine et al. (73). Briefly, polymerized microtubules and Alexa 488-labeled Tau constructs were incubated for 20 min at 25°C in pelleting buffer (BRB80, 1 mM dithiothreitol, 10 $\mu\text{g}/\text{mL}$ bovine serum albumin [BSA], pH 6.9) with the addition of 10 μM paclitaxel (Sigma Aldrich) for Taxol microtubules in BSA-coated tubes. The reactions were centrifuged in a TLA-100 rotor in an Optima TLX Ultracentrifuge (Beckman). The supernatant was removed, and the pellet was resuspended in ice-cold BRB80 with 10 mg/mL BSA. Fluorescence was measured using a fluorometer (Photon Technology International) with an excitation of 493 nm and an emission of 517 nm. *SI Appendix, Supplementary Information Text* has details.

TIRF Microscopy. TIRF microscopy experiments were carried out at room temperature using an inverted Eclipse Ti-E microscope (Nikon) with 100 \times Apo TIRF objective lens (1.49 numerical aperture) and dual iXon Ultra Electron Multiplying charge-coupled device cameras running NIS Elements, version 4.51.0. Tau binding assays were completed as previously described with Alexa 488-labeled microtubules and Alexa 647-labeled Tau constructs (43). TIRF dynamics assays using low concentrations of Tau were done as described (43) using Alexa 488 microtubules and Alexa 647-labeled Tau. Three color-spiking experiments examining dynamics at high concentrations of Tau were performed using Alexa 405 microtubules and high concentrations of Alexa 488-labeled Tau spiked with 300 pM Alexa 647-labeled Tau. *SI Appendix, Supplementary Information Text* has details.

CD. CD spectra of 10 μM WT-Tau and R5L-Tau were acquired on a Chirascan (Applied Photophysics) spectrometer. *SI Appendix, Supplementary Information Text* has details.

NMR Spectroscopy. NMR experiments were performed on a Bruker 700-MHz spectrometer equipped with a cryogenic probe. The 2D ^1H - ^{15}N HSQC experiments were recorded at 5°C on 10 μM ^{15}N -labeled Tau in BRB80 buffer and 10% D_2O in the absence or presence of 20 μM Taxol microtubules. For the sequence-specific resonance assignment of the peptide (residues 1 to 20 of Tau), natural abundance 2D ^1H - ^{15}N HSQC, 2D ^1H - ^1H total correlation spectroscopy (TOCSY), and 2D ^1H - ^1H nuclear Overhauser effect spectroscopy were recorded at 5°C on 2 mM samples in BRB80 buffer and 10% D_2O . STD experiments were recorded using the Bruker pulse sequence stdifggp19.2 with 5 μM Taxol microtubules and peptides concentrations from 50 μM to 2 mM. *SI Appendix, Supplementary Information Text* has details.

Data Availability. All study data are included in the article and/or supporting information.

ACKNOWLEDGMENTS. We thank David Warshaw and Guy Kennedy for training and support of the TIRF microscope at the University of Vermont and Vermont Livestock Slaughter & Processing (Ferrisburgh, VT) for supporting our work. This work was supported by the NIH, National Institute of General Medical Sciences Grant GM132646 (to A.G.H. and C.L.B.). M.Z. was supported by Deutsche Forschungsgemeinschaft (German Research Foundation) Grants SFB 860 and TP B2 and European Research Council European Union Horizon 2020 Research and Innovation Programme Grant 787679.

1. D. Panda, J. C. Samuel, M. Massie, S. C. Feinstein, L. Wilson, Differential regulation of microtubule dynamics by three- and four-repeat tau: Implications for the onset of neurodegenerative disease. *Proc. Natl. Acad. Sci. U.S.A.* **100**, 9548–9553 (2003).
2. D. B. Murphy, K. A. Johnson, G. G. Borisy, Role of tubulin-associated proteins in microtubule nucleation and elongation. *J. Mol. Biol.* **117**, 33–52 (1977).
3. G. J. Hoeprich, A. R. Thompson, D. P. McVicker, W. O. Hancock, C. L. Berger, Kinesin's neck-linker determines its ability to navigate obstacles on the microtubule surface. *Biophys. J.* **106**, 1691–1700 (2014).
4. D. P. McVicker, L. R. Chrin, C. L. Berger, The nucleotide-binding state of microtubules modulates kinesin processivity and the ability of tau to inhibit kinesin-mediated transport. *J. Biol. Chem.* **286**, 42873–42880 (2011).
5. M. Verzhinin, B. C. Carter, D. S. Razafsky, S. J. King, S. P. Gross, Multiple-motor based transport and its regulation by tau. *Proc. Natl. Acad. Sci. U.S.A.* **104**, 87–92 (2007).
6. R. Dixit, J. L. Ross, Y. E. Goldman, E. L. Holzbaur, Differential regulation of dynein and kinesin motor proteins by tau. *Science* **319**, 1086–1089 (2008).
7. N. M. Kanaan et al., Phosphorylation in the amino terminus of tau prevents inhibition of anterograde axonal transport. *Neurobiol. Aging* **33**, 826.e15–826.e30 (2012).

8. N. M. Kanaan et al., Pathogenic forms of tau inhibit kinesin-dependent axonal transport through a mechanism involving activation of axonal phosphotransferases. *J. Neurosci.* **31**, 9858–9868 (2011).
9. I. Grundke-Iqbal et al., Microtubule-associated protein tau. A component of Alzheimer paired helical filaments. *J. Biol. Chem.* **261**, 6084–6089 (1986).
10. B. Borroni et al., Tau forms in CSF as a reliable biomarker for progressive supranuclear palsy. *Neurology* **71**, 1796–1803 (2008).
11. B. Borroni et al., Tau haplotype influences cerebral perfusion pattern in frontotemporal lobar degeneration and related disorders. *Acta Neurol. Scand.* **117**, 359–366 (2008).
12. M. Goedert, C. M. Wischik, R. A. Crowther, J. E. Walker, A. Klug, Cloning and sequencing of the cDNA encoding a core protein of the paired helical filament of Alzheimer disease: Identification as the microtubule-associated protein tau. *Proc. Natl. Acad. Sci. U.S.A.* **85**, 4051–4055 (1988).
13. C. M. Wischik et al., Isolation of a fragment of tau derived from the core of the paired helical filament of Alzheimer disease. *Proc. Natl. Acad. Sci. U.S.A.* **85**, 4506–4510 (1988).

14. G. Lindwall, R. D. Cole, Phosphorylation affects the ability of tau protein to promote microtubule assembly. *J. Biol. Chem.* **259**, 5301–5305 (1984).
15. E. M. Mandelkow et al., Tau domains, phosphorylation, and interactions with microtubules. *Neurobiol. Aging* **16**, 355–362 (1995).
16. B. Zhang et al., Microtubule-binding drugs offset tau sequestration by stabilizing microtubules and reversing fast axonal transport deficits in a tauopathy model. *Proc. Natl. Acad. Sci. U.S.A.* **102**, 227–231 (2005).
17. M. Goedert, Tau gene mutations and their effects. *Mov. Disord.* **20** (suppl. 12), S45–S52 (2005).
18. K. H. Strang, T. E. Golde, B. I. Giasson, MAPT mutations, tauopathy, and mechanisms of neurodegeneration. *Lab. Invest.* **99**, 912–928 (2019).
19. M. D. Weingarten, A. H. Lockwood, S. Y. Hwo, M. W. Kirschner, A protein factor essential for microtubule assembly. *Proc. Natl. Acad. Sci. U.S.A.* **72**, 1858–1862 (1975).
20. J. Avila, J. J. Lucas, M. Perez, F. Hernandez, Role of tau protein in both physiological and pathological conditions. *Physiol. Rev.* **84**, 361–384 (2004).
21. B. L. Goode, M. Chau, P. E. Denis, S. C. Feinstein, Structural and functional differences between 3-repeat and 4-repeat tau isoforms. Implications for normal tau function and the onset of neurodegenerative disease. *J. Biol. Chem.* **275**, 38182–38189 (2000).
22. M. Goedert, M. G. Spillantini, R. Jakes, D. Rutherford, R. A. Crowther, Multiple isoforms of human microtubule-associated protein tau: Sequences and localization in neurofibrillary tangles of Alzheimer's disease. *Neuron* **3**, 519–526 (1989).
23. H. Kadavath et al., Folding of the tau protein on microtubules. *Angew. Chem. Int. Ed. Engl.* **54**, 10347–10351 (2015).
24. M. D. Mukrasch et al., The “jaws” of the tau-microtubule interaction. *J. Biol. Chem.* **282**, 12230–12239 (2007).
25. H. Kadavath et al., Tau stabilizes microtubules by binding at the interface between tubulin heterodimers. *Proc. Natl. Acad. Sci. U.S.A.* **112**, 7501–7506 (2015).
26. B. L. Goode et al., Functional interactions between the proline-rich and repeat regions of tau enhance microtubule binding and assembly. *Mol. Biol. Cell* **8**, 353–365 (1997).
27. N. Gustke, B. Trinczek, J. Biernat, E. M. Mandelkow, E. Mandelkow, Domains of tau protein and interactions with microtubules. *Biochemistry* **33**, 9511–9522 (1994).
28. B. Trinczek, J. Biernat, K. Baumann, E. M. Mandelkow, E. Mandelkow, Domains of tau protein, differential phosphorylation, and dynamic instability of microtubules. *Mol. Biol. Cell* **6**, 1887–1902 (1995).
29. E. H. Kellogg et al., Near-atomic model of microtubule-tau interactions. *Science* **360**, 1242–1246 (2018).
30. K. M. McKibben, E. Rhoades, Independent tubulin binding and polymerization by the proline-rich region of tau is regulated by tau's N-terminal domain. *J. Biol. Chem.* **294**, 19381–19394 (2019).
31. A. M. Melo et al., A functional role for intrinsic disorder in the tau-tubulin complex. *Proc. Natl. Acad. Sci. U.S.A.* **113**, 14336–14341 (2016).
32. M. H. Hinrichs et al., Tau protein diffuses along the microtubule lattice. *J. Biol. Chem.* **287**, 38559–38568 (2012).
33. D. P. McVicker, G. J. Hoepflich, A. R. Thompson, C. L. Berger, Tau interconverts between diffusive and stable populations on the microtubule surface in an isoform and lattice specific manner. *Cytoskeleton (Hoboken)* **71**, 184–194 (2014).
34. V. Siahhaan et al., Kinetically distinct phases of tau on microtubules regulate kinesin motors and severing enzymes. *Nat. Cell Biol.* **21**, 1086–1092 (2019).
35. R. Tan et al., Microtubules gate tau condensation to spatially regulate microtubule functions. *Nat. Cell Biol.* **21**, 1078–1085 (2019).
36. M. T. Gyparakis et al., Tau forms oligomeric complexes on microtubules that are distinct from tau aggregates. *Proc. Natl. Acad. Sci. U.S.A.* **118**, e2021461118 (2021).
37. A. Deshpande, K. M. Win, J. Busciglio, Tau isoform expression and regulation in human cortical neurons. *FASEB J.* **22**, 2357–2367 (2008).
38. P. Poorkaj et al., An R5L tau mutation in a subject with a progressive supranuclear palsy phenotype. *Ann. Neurol.* **52**, 511–516 (2002).
39. Y. Mutreja, B. Combs, T. C. Gambin, FTDP-17 mutations alter the aggregation and microtubule stabilization propensity of tau in an isoform-specific fashion. *Biochemistry* **58**, 742–754 (2019).
40. P. Poorkaj et al., Tau is a candidate gene for chromosome 17 frontotemporal dementia. *Ann. Neurol.* **43**, 815–825 (1998).
41. B. L. Goode, S. C. Feinstein, Identification of a novel microtubule binding and assembly domain in the developmentally regulated inter-repeat region of tau. *J. Cell Biol.* **124**, 769–782 (1994).
42. K. A. Butner, M. W. Kirschner, Tau protein binds to microtubules through a flexible array of distributed weak sites. *J. Cell Biol.* **115**, 717–730 (1991).
43. J. L. Stern, D. V. Lessard, G. J. Hoepflich, G. A. Morfini, C. L. Berger, Phosphoregulation of Tau modulates inhibition of kinesin-1 motility. *Mol. Biol. Cell* **28**, 1079–1087 (2017).
44. A. R. Duan et al., Interactions between tau and different conformations of tubulin: Implications for tau function and mechanism. *J. Mol. Biol.* **429**, 1424–1438 (2017).
45. B. T. Castle, K. M. McKibben, E. Rhoades, D. J. Odde, Tau avoids the GTP cap at growing microtubule plus-ends. *iScience* **23**, 101782 (2020).
46. S. M. Kelly, T. J. Jess, N. C. Price, How to study proteins by circular dichroism. *Biochim. Biophys. Acta* **1751**, 119–139 (2005).
47. S. Kosol, S. Contreras-Martos, C. Cedeño, P. Tompa, Structural characterization of intrinsically disordered proteins by NMR spectroscopy. *Molecules* **18**, 10802–10828 (2013).
48. M. D. Mukrasch et al., Structural polymorphism of 441-residue tau at single residue resolution. *PLoS Biol.* **7**, e34 (2009).
49. M. Mayer, B. Meyer, Characterization of ligand binding by saturation transfer difference NMR spectroscopy. *Angew. Chem. Int. Ed. Engl.* **38**, 1784–1788 (1999).
50. S. Walpole, S. Monaco, R. Nepravishta, J. Angulo, STD NMR as a technique for ligand screening and structural studies. *Methods Enzymol.* **615**, 423–451 (2019).
51. H. Kadavath et al., The binding mode of a tau peptide with tubulin. *Angew. Chem. Int. Ed. Engl.* **57**, 3246–3250 (2018).
52. S. Barghorn et al., Structure, microtubule interactions, and paired helical filament aggregation by tau mutants of frontotemporal dementias. *Biochemistry* **39**, 11714–11721 (2000).
53. I. D'Souza et al., Missense and silent tau gene mutations cause frontotemporal dementia with parkinsonism-chromosome 17 type, by affecting multiple alternative RNA splicing regulatory elements. *Proc. Natl. Acad. Sci. U.S.A.* **96**, 5598–5603 (1999).
54. M. Hong et al., Mutation-specific functional impairments in distinct tau isoforms of hereditary FTDP-17. *Science* **282**, 1914–1917 (1998).
55. M. Hasegawa, M. J. Smith, M. Goedert, Tau proteins with FTDP-17 mutations have a reduced ability to promote microtubule assembly. *FEBS Lett.* **437**, 207–210 (1998).
56. P. Rizzu et al., Mutation-dependent aggregation of tau protein and its selective depletion from the soluble fraction in brain of P301L FTDP-17 patients. *Hum. Mol. Genet.* **9**, 3075–3082 (2000).
57. S. Jeganathan, M. von Bergen, H. Brutlach, H. J. Steinhoff, E. Mandelkow, Global hairpin folding of tau in solution. *Biochemistry* **45**, 2283–2293 (2006).
58. M. Schwalbe et al., Predictive atomic resolution descriptions of intrinsically disordered hTau40 and α -synuclein in solution from NMR and small angle scattering. *Structure* **22**, 238–249 (2014).
59. K. J. Rosenber, J. L. Ross, H. E. Feinstein, S. C. Feinstein, J. Israelachvili, Complementary dimerization of microtubule-associated tau protein: Implications for microtubule bundling and tau-mediated pathogenesis. *Proc. Natl. Acad. Sci. U.S.A.* **105**, 7445–7450 (2008).
60. M. Schwalbe et al., Structural impact of tau phosphorylation at threonine 231. *Structure* **23**, 1448–1458 (2015).
61. H. E. Feinstein et al., Oligomerization of the microtubule-associated protein tau is mediated by its N-terminal sequences: Implications for normal and pathological tau action. *J. Neurochem.* **137**, 939–954 (2016).
62. N. Hirokawa, Y. Shiomura, S. Okabe, Tau proteins: The molecular structure and mode of binding on microtubules. *J. Cell Biol.* **107**, 1449–1459 (1988).
63. L. Balabanian, C. L. Berger, A. G. Hendricks, Acetylated microtubules are preferentially bundled leading to enhanced kinesin-1 motility. *Biophys. J.* **113**, 1551–1560 (2017).
64. A. R. Chaudhary, F. Berger, C. L. Berger, A. G. Hendricks, Tau directs intracellular trafficking by regulating the forces exerted by kinesin and dynein teams. *Traffic* **19**, 111–121 (2018).
65. C. L. Berger, D. V. Lessard, The microtubule associated protein tau regulates KIF1A pausing behavior and motility. *bioRxiv [Preprint]* (2021). 10.1101/2021.08.11.455914 (Accessed 12 August 2021).
66. P. J. Hooikaas et al., MAP7 family proteins regulate kinesin-1 recruitment and activation. *J. Cell Biol.* **218**, 1298–1318 (2019).
67. B. Y. Monroy et al., Competition between microtubule-associated proteins directs motor transport. *Nat. Commun.* **9**, 1487 (2018).
68. J. Chen, Y. Kanai, N. J. Cowan, N. Hirokawa, Projection domains of MAP2 and tau determine spacings between microtubules in dendrites and axons. *Nature* **360**, 674–677 (1992).
69. G. Simić et al., Tau protein hyperphosphorylation and aggregation in Alzheimer's disease and other tauopathies, and possible neuroprotective strategies. *Biomolecules* **6**, 6 (2016).
70. T. C. Gambin et al., In vitro polymerization of tau protein monitored by laser light scattering: Method and application to the study of FTDP-17 mutants. *Biochemistry* **39**, 6136–6144 (2000).
71. E. Chang, S. Kim, H. Yin, H. N. Nagaraja, J. Kuret, Pathogenic missense MAPT mutations differentially modulate tau aggregation propensity at nucleation and extension steps. *J. Neurochem.* **107**, 1113–1123 (2008).
72. M. Castoldi, A. V. Popov, Purification of brain tubulin through two cycles of polymerization-depolymerization in a high-molarity buffer. *Protein Expr. Purif.* **32**, 83–88 (2003).
73. R. A. Charafeddine et al., Tau repeat regions contain conserved histidine residues that modulate microtubule-binding in response to changes in pH. *J. Biol. Chem.* **294**, 8779–8790 (2019).